# Effect of Substrate Dielectric Anisotropy on the Frequency Behavior of Microstrip Circuits

Enrique Drake, Rafael R. Boix, *Member, IEEE*, Manuel Horno, *Member, IEEE*, and Tapan K. Sarkar, *Fellow, IEEE*

***Abstract*—In this paper, we carry out a full-wave analysis of shielded two-port microstrip circuits, in which the metallizations are embedded in a multilayered substrate that may contain isotropic dielectrics and/or anisotropic dielectrics. The Galerkin's method in the spectral domain is applied for determining the current density on the metallizations of the circuits when their feeding lines are excited by means of delta-gap generators, and the matrix pencil technique is subsequently used for deembedding the scattering parameters from the computed current densities. Results are presented for the scattering parameters of some microstrip discontinuities and filters printed on both isotropic dielectric substrates and anisotropic dielectric substrates. These results show that when substrate dielectric anisotropy is ignored, errors arise when computing the scattering parameters of microstrip discontinuities and when predicting the operating frequency band of microstrip filters.**

***Index Terms*—Anisotropic dielectric substrates, microstrip circuits, spectral-domain numerical techniques.**

## I. Introduction

MICROSTRIP configurations fabricated in multilayered substrates with different metallization planes offer the advantage of greater compactness and increased versatility over conventional microstrip configurations fabricated on one-layered substrates. These multilayered microstrip configurations have been successfully used in the last few years for the design of passive microwave integrated circuits (MIC's) such as bandpass filters [1]–[3], directional couplers [1], and dc-block high-frequency transitions [1], [4]. Aside from the applications of multilayered microstrip structures, it has been reported that some of the standard materials used as substrates of MIC's exhibit a certain degree of dielectric anisotropy, which either is a consequence of the cristalline nature of the material (sapphire, pyrolitic–boron–nitride) or is introduced during the manufacturing process (woven glass PTFE, Epsilam-10) [5]. Since the performance of both microstrip circuits and microstrip antennas strongly depends on the features of the substrates, dielectric anisotropy should be fully and accurately accounted for whenever it is present [5], [6]. In fact, in some cases, the presence of dielectric anisotropy has been found to have a beneficial effect on circuit performance as it happens with the design of high-directivity microstrip directional couplers printed on anisotropic dielectric substrates [5].

In this paper, the authors present a full-wave algorithm for the determination of the scattering parameters of one- and two-port shielded microstrip circuits in the case in which the metallizations of the circuits occupy one or two interfaces of a multilayered substrate containing anisotropic dielectrics. Although there is an abundant bibliography concerning the analysis of microstrip transmission lines on anisotropic dielectric substrates (see [5], [7]), as far as the authors know, there are few references dealing with the analysis of microstrip circuits—including microstrip discontinuities—on anisotropic dielectric substrates [8]. As an example, in [9] and [10], a method is presented for the determination of the quasi-static capacitive equivalent circuits of microstrip open-end discontinuities, microstrip gap discontinuities, and microstrip crossover discontinuities embedded in multilayered substrates with dielectric anisotropy. Toncich *et al.* [11] present a full-wave method-of-moments approach for the characterization of open-end microstrip discontinuities printed on anisotropic dielectric layers. Chen and Becker [8] apply the method of lines and the transverse resonance technique to the determination of the frequency-dependent scattering parameters of microstrip step discontinuities printed on layers that may exhibit both dielectric and magnetic anisotropy. Finally, Goswami *et al.* [12] use a full-wave method of moments in the spectral domain for the characterization of single and coupled microstrip open-ended discontinuities printed on anisotropic dielectric layers. In this latter paper, the discontinuities are analyzed in an open environment and radiation effects are accounted for. In this paper, focus is placed on analyzing how the presence of dielectric anisotropy affects both the frequency behavior of some microstrip discontinuities and some simple bandpass microstrip filters. In Section II of this paper, the authors briefly describe the numerical procedure used for obtaining the scattering parameters of the microstrip circuits analyzed. Galerkin's method in the spectral domain is used for determining the current density excited on the metallizations of the circuits by delta-gap voltage generators, and the matrix pencil technique is subsequently applied for deembedding the scattering parameters from the computed current densities. In Section III, we present numerical results obtained with the algorithm described in Section II. On one hand, our numerical

Manuscript received October 7, 1998. This work was supported by the Comisión Interministerial de Ciencia y Tecnología, Spain under Project TIC98-0630.

E. Drake is with the Microwave Group, Department of Applied Physics, School of Industrial and Telecommunications Engineering, University of Seville, 41092 Seville, Spain.

R. R. Boix is with the Microwaves Group, Department of Electronics and Electromagnetism, School of Physics, University of Seville, 41012 Seville, Spain (e-mail: boix@cica.es).

M. Horno, deceased, was with the Microwaves Group, Department of Electronics and Electromagnetism, School of Physics, University of Seville, 41012 Seville, Spain.

T. K. Sarkar is with the Department of Electrical and Computer Engineering, Syracuse University, Syracuse, NY 13244 USA.

Publisher Item Identifier S 0018-9480(00)06542-X.

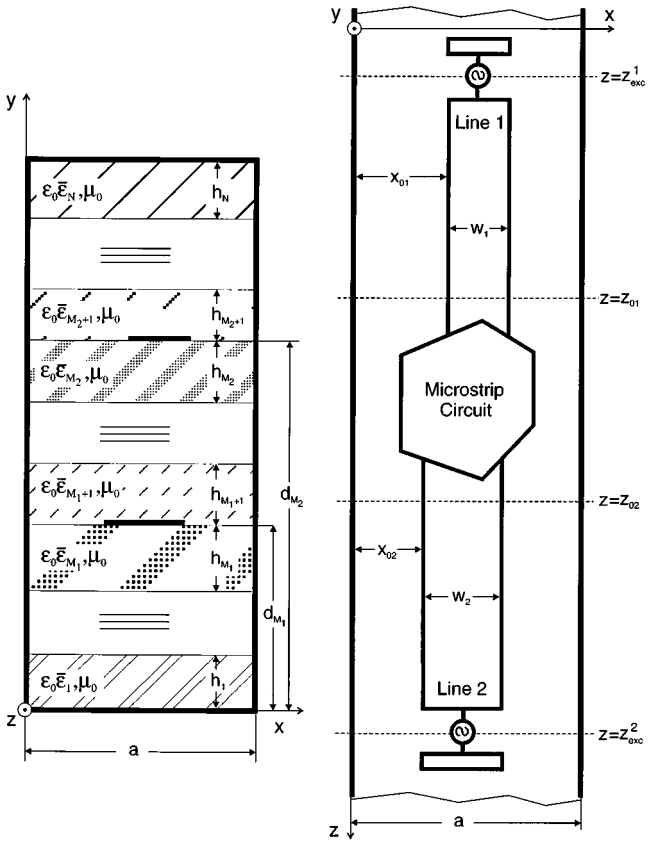


Fig. 1. Side (a) and top (b) views of two-port microstrip circuit embedded in a multilayered substrate with dielectric anisotropy.

results are compared with previously published results, and a good agreement is found in all cases. On the other hand, original numerical results are shown for microstrip discontinuities and filters fabricated on anisotropic dielectric substrates, and these results are compared in all cases with the results that would be obtained if dielectric anisotropy were neglected.

## II. Formulation of the Problem and Numerical Procedure

### A. Two-Port Microstrip Circuit

Fig. 1 shows the side and top views of the type of two-port microstrip circuit analyzed in this paper. This microstrip circuit is fed by two microstrip transmission lines, which are excited by delta-gap voltage generators placed at the excitation planes $z = z^1_{\rm exc}$ and $z = z^2_{\rm exc}$ [13], [3]. As shown in Fig. 1(b), the two feeding microstrip lines are left open at the excitation ends, as in [13]. The metallizations of the circuit and feeding lines are considered to be perfect electric conductors (PEC's) of neglecting thickness. Without loss of generality, it is assumed that the metallic strip of feeding line 1 is placed at the plane $y = d_{M_1}$ and that of line 2 is placed at the plane $y = d_{M_2}$ (the study carried out below in this section can be trivially extended to the case in which the two metallic strips of the feeding lines are placed at a common plane, which is a situation encountered in the results section), and that the metallizations of the circuit may occupy both planes $y = d_{M_1}$ and $y = d_{M_2}$. Looking at Fig. 1(a), this means that the metallizations of the feeding lines as well as the metallizations of the circuit generally occupy two of the interfaces of a stratified substrate, which is assumed to be compounded of lossless isotropic dielectric layers and/or lossless anisotropic dielectric layers [see Fig. 1(a)]. The whole multilayered substrate containing the metallizations is placed within a shielding rectangular waveguide with walls that are considered to be PEC's, and both the substrate and shielding waveguide are assumed to be of infinite extent all along the $z$-coordinate (as in [14]). Finally, it is also assumed that the permittivity tensor of the $i$th layer of the multilayered substrate $(i = 1, \cdots, N)$ is a diagonal tensor of the form (in [7, eq. (1)])

$$\epsilon_0 \overline{\epsilon}_i = \epsilon_0 \begin{pmatrix} \epsilon^i_{xx} & 0 & 0 \\ 0 & \epsilon^i_{yy} & 0 \\ 0 & 0 & \epsilon^i_{zz} \end{pmatrix}. \tag{1}$$

Depending on the relations existing among the values of $\epsilon^i_{xx}$, $\epsilon^i_{yy}$, and $\epsilon^i_{zz}$ in (1), the $i$th layer $(i = 1, \cdots, N)$ of the multilayered substrate of Fig. 1(a) will behave as any one of the three following possibilities: an isotropic dielectric, an uniaxial anisotropic dielectric, and a biaxial anisotropic dielectric [5].

Although the analysis of shielded microstrip circuits has been traditionally carried out by enclosing the whole circuit inside a metallic rectangular cavity [15], [16], in this paper, the shielded microstrip circuits studied are placed within a rectangular waveguide of infinite extent in the axial direction [the $z$-direction in Fig. 1(a) and (b)]. By comparison with the approach followed in [15] and [16], the approach followed in this paper has the advantage that cavity resonances do not affect the performance of the circuits analyzed [16].

### B. Determination of the Current Density Via Galerkin's Method in the Spectral Domain

In order to obtain the scattering parameters of the two-port microstrip circuit of Fig. 1(a) and (b), it is necessary to obtain the surface current density on the metallizations of the circuit and the feeding transmission lines. Let $\boldsymbol{j}(x, y = d_{M_j}, z)(j = 1, 2)$ be the surface current density existing on the metallized surface $S_j (j = 1, 2)$ of the plane $y = d_{M_j} (j = 1, 2)$ inside the multilayered structure of Fig. 1(a). By imposing the boundary conditions that the total tangential electric field is zero on $S_1$ and $S_2$, a set of two coupled electric-field integral equations (EFIE's) is obtained for the two functions $\boldsymbol{j}(x, y = d_{M_1}, z)$ and $\boldsymbol{j}(x, y = d_{M_2}, z)$. This set of coupled integral equations can be written as

$$\begin{aligned} &\boldsymbol{E}_t(x, y = d_{M_i}, z) \\ &\quad = \boldsymbol{E}_{t,\rm exc}(x, y = d_{M_i}, z) \\ &\qquad + \sum_{j=1}^{2} \int_{S'_j} \overline{\boldsymbol{G}}_t(x, x', y = d_{M_i}, y' = d_{M_j}, z - z') \\ &\qquad \cdot \boldsymbol{j}(x', y' = d_{M_j}, z')\, dx' dz' = \boldsymbol{0}, \\ &\qquad (x, y = d_{M_i}, z) \in S_i; \quad i = 1, 2 \end{aligned} \tag{2}$$

where $\boldsymbol{E}_{t,\,\rm exc}(x, y = d_{M_i}, z)(i = 1, 2)$ is the tangential excitation electric field introduced by the delta-gap voltage gen-

erator connected to the $i$th $(i = 1, 2)$ feeding line [17] and $\overline{\boldsymbol{G}}_t(x, x', y, y', z - z')$ is the transverse dyadic Green's function relating the tangential electric field and current density [18] inside the multilayered substrate of Fig. 1(a). This transverse dyadic Green's function is a $2 \times 2$ matrix.

In this paper, the two unknown functions $\boldsymbol{j}(x, y = d_{M_1}, z)$ and $\boldsymbol{j}(x, y = d_{M_2}, z)$ are obtained by solving the set of two integrals equations shown in (2) via the Galerkin's method. As a first step, these two unknown functions are expressed as a linear combination of known basis functions $\boldsymbol{j}_{jl}(x, z)(j = 1, 2;\ l = 1, \cdots, N_j)$ as follows:

$$\boldsymbol{j}(x, y = d_{M_j}, z) = \sum_{l=1}^{N_j} a_{jl}\boldsymbol{j}_{jl}(x, z), \qquad j = 1, 2 \tag{3}$$

where $a_{jl}(j = 1, 2;\ l = 1, \cdots, N_j)$ are unknown coefficients of basis functions. In order to determine these unknown coefficients, a standard Galerkin's procedure is followed and the inner product is taken between every basis function of (3) (now acting as a testing function) and the resulting equations of substituting (3) into (2). As a consequence of this operation, a system of linear equations is obtained for the unknown coefficients $a_{jl}(j = 1, 2;\ l = 1, \cdots, N_j)$. This system of equations can be written as

$$\sum_{j=1}^{2}\sum_{l=1}^{N_j} \Gamma_{jl}^{ik} a_{jl} = b_{ik}, \qquad i = 1, 2;\ k = 1, \cdots, N_i \tag{4}$$

where

$$\begin{aligned}\Gamma_{jl}^{ik} = &\int_{S_i}\int_{S_j'} \left[\boldsymbol{j}_{ik}^*(x, z)\right]^t \\ &\cdot \overline{\boldsymbol{G}}_t(x, x', y = d_{M_i}, y' = d_{M_j}, z - z') \\ &\cdot \boldsymbol{j}_{jl}(x', z')\, dx'dz'dxdz, \qquad i, j = 1, 2; \\ &\qquad k = 1, \cdots, N_i;\ l = 1, \cdots, N_j\end{aligned} \tag{5}$$

and

$$\begin{aligned}b_{ik} = -\int_{S_i} \left[\boldsymbol{j}_{ik}^*(x, z)\right]^t \cdot \boldsymbol{E}_{t,\mathrm{exc}}(x, y = d_{M_i}, z)\, dxdz, \\ i = 1, 2;\ k = 1, \cdots, N_i.\end{aligned} \tag{6}$$

Once $\Gamma_{jl}^{ik}(i, j = 1, 2;\ k = 1, \cdots, N_i;\ l = 1, \cdots, N_j)$ and $b_{ik}(i = 1, 2;\ k = 1, \cdots, N_i)$ are known, the system of equations (4) can be solved for obtaining the unknown coefficients of basis functions $a_{jl}(j = 1, 2;\ l = 1, \cdots, N_j)$. In general, the numerical determination of the four-dimensional integrals appearing in (5) requires to determine the elements of $\overline{\boldsymbol{G}}_t(x, x', y = d_{M_i}, y' = d_{M_j}, z - z')(i, j = 1, 2)$ for a high number of different values of $x$, $x'$, $z$, and $z'$. Also, the computation of the elements of $\overline{\boldsymbol{G}}_t(x, x', y = d_{M_i}, y' = d_{M_j}, z - z')(i, j = 1, 2)$ requires to work out infinite summations of infinite integrals [see (8)–(11)] for every particular set of values of $x$, $x'$, $z$, and $z'$. All this implies that the direct computation of $\Gamma_{jl}^{ik}(i, j = 1, 2;\ k = 1, \cdots, N_i;\ l = 1, \cdots, N_j)$ via (5) may lead to prohibitive central processing unit (CPU) times. With a view to avoiding this problem, in this paper, the computation of $\Gamma_{jl}^{ik}(i, j = 1, 2;\ k = 1, \cdots, N_i;\ l = 1, \cdots, N_j)$ is carried out via an alternative expression in the spectral domain, which is equivalent to (5). In order to obtain that expression, it is firstly taken into account that the structure of Fig. 1(a) together with its image through the electric wall $x = 0$ constitute a periodic structure along the $x$-coordinate of period $2a$, and bearing in mind this idea, Parseval's theorem is applied to the integrals of (5). As a result of this operation, it can be shown that the expression of $\Gamma_{jl}^{ik}(i, j = 1, 2;\ k = 1, \cdots, N_i;\ l = 1, \cdots, N_j)$ in the spectral domain used in this paper is given by (see [14] and [19])

$$\begin{aligned}\Gamma_{jl}^{ik} = \frac{a}{2\pi}\sum_{n=-\infty}^{+\infty}\int_{-\infty}^{+\infty} &\left[\tilde{\boldsymbol{j}}_{ik}^*(n, k_z)\right]^t \\ &\cdot \tilde{\overline{\boldsymbol{G}}}_t(n, y = d_{M_i}, y' = d_{M_j}, k_z) \cdot \tilde{\boldsymbol{j}}_{jl}(n, k_z)\, dk_z, \\ &i, j = 1, 2;\ k = 1, \cdots, N_i;\ l = 1, \cdots, N_j\end{aligned} \tag{7}$$

where $\tilde{\overline{\boldsymbol{G}}}_t(n, y, y', k_z)$ is a $2 \times 2$ matrix, which stands for the spectral transverse dyadic Green's function. The elements of this matrix, $\tilde{G}_{t,rs}(n, y, y', k_z)(r, s = x, z)$ are related to the elements of $\overline{\boldsymbol{G}}_t(x, x', y, y', z - z')$, $G_{t,rs}(x, x', y, y', z - z')(r, s = x, z)$ via the following set of equations:

$$\begin{aligned}&G_{t,xx}(x, x', y, y', z - z') \\ &\quad = \frac{2}{a\pi}\sum_{n=1}^{+\infty}\int_0^{+\infty} \tilde{G}_{t,xx}(n, y, y', k_z)\cos\left(\frac{n\pi x}{a}\right) \\ &\qquad \cdot \cos\left(\frac{n\pi x'}{a}\right)\cos\left(k_z(z - z')\right)dk_z \\ &\qquad + \frac{1}{a\pi}\int_0^{+\infty} \tilde{G}_{t,xx}(n = 0, y, y', k_z) \\ &\qquad \cdot \cos\left(k_z(z - z')\right)dk_z\end{aligned} \tag{8}$$

$$\begin{aligned}&G_{t,zx}(x, x', y, y', z - z') \\ &\quad = -\frac{2}{a\pi}\sum_{n=1}^{+\infty}\int_0^{+\infty} \tilde{G}_{t,zx}(n, y, y', k_z)\sin\left(\frac{n\pi x}{a}\right) \\ &\qquad \cdot \cos\left(\frac{n\pi x'}{a}\right)\sin\left(k_z(z - z')\right)dk_z\end{aligned} \tag{9}$$

$$\begin{aligned}&G_{t,xz}(x, x', y, y', z - z') \\ &\quad = \frac{2}{a\pi}\sum_{n=1}^{+\infty}\int_0^{+\infty} \tilde{G}_{t,xz}(n, y, y', k_z)\cos\left(\frac{n\pi x}{a}\right) \\ &\qquad \cdot \sin\left(\frac{n\pi x'}{a}\right)\sin\left(k_z(z - z')\right)dk_z\end{aligned} \tag{10}$$

$$\begin{aligned}&G_{t,zz}(x, x', y, y', z - z') \\ &\quad = \frac{2}{a\pi}\sum_{n=1}^{+\infty}\int_0^{+\infty} \tilde{G}_{t,zz}(n, y, y', k_z)\sin\left(\frac{n\pi x}{a}\right) \\ &\qquad \cdot \sin\left(\frac{n\pi x'}{a}\right)\cos\left(k_z(z - z')\right)dk_z.\end{aligned} \tag{11}$$

As stated before, the computation of the elements of $\overline{\boldsymbol{G}}_t(x, x', y, y', z - z')$ for the multilayered anisotropic substrate of Fig. 1(a) is very awkward and has to be necessarily carried out via (8)–(11) [14]. However, the computation of the elements of $\tilde{\overline{\boldsymbol{G}}}_t(n, y, y', k_z)$ for the substrate of Fig. 1(a) can be carried out in a very straightforward way [14]. In this paper, the recurrent algorithm described in [7] has been used for computing the elements of $\tilde{\overline{\boldsymbol{G}}}_t(n, y, y', k_z)$ needed in (7) in

those cases in which the source and field points lie at the same dielectric interface (i.e., when $y = y' = d_{M_i} (i = 1, 2)$). Also, an extension of the algorithm of [7] based on the equivalent boundary method [20] has been used for computing the elements of $\overline{\tilde{\boldsymbol{G}}}_t(n, y, y', k_z)$ needed in (7) in the cases in which the source and field points lie at different dielectric interfaces (i.e., when $y \neq y'$).

Concerning the functions $\tilde{\boldsymbol{j}}_{jl}(n, k_z)(j = 1, 2;\ l = 1, \cdots, N_j)$ shown in (7), these functions stand for the spectral versions of the basis functions $\boldsymbol{j}_{jl}(x, z)(j = 1, 2;\ l = 1, \cdots, N_j)$, and they can be obtained by using the following:

$$\tilde{\boldsymbol{j}}_{jl}(n, k_z) = \frac{1}{2a} \int_{-a}^{a} \int_{-\infty}^{\infty} \boldsymbol{j}_{jl}^{\text{ext}}(x, z) e^{j((n\pi x/a) + k_z z)}\, dz dx, \quad j = 1, 2;\ l = 1, \cdots, N_j \tag{12}$$

where $\boldsymbol{j}_{jl}^{\text{ext}}(x, z)(j = 1, 2;\ l = 1, \cdots, N_j)$ is an extension of the basis function $\boldsymbol{j}_{jl}(x, z)(j = 1, 2;\ l = 1, \cdots, N_j)$ to the interval $-a \leq x \leq +a$, which consists of that basis function together with its image through the electric wall $x = 0$ (i.e., $\boldsymbol{j}_{jl}^{\text{ext}}(x, z) = \boldsymbol{j}_{jl}(x, z) = j_{jl,x}(x, z)\hat{\boldsymbol{x}} + j_{jl,z}(x, z)\hat{\boldsymbol{z}}$ if $0 \leq x \leq +a$ and $\boldsymbol{j}_{jl}^{\text{ext}}(x, z) = j_{jl,x}(-x, z)\hat{\boldsymbol{x}} - j_{jl,z}(-x, z)\hat{\boldsymbol{z}}$ if $-a \leq x \leq 0$).

The basis functions chosen in this paper for approximating the current density on the metallizations of the structure of Fig. 1(a) and (b) [see (3)] are rooftop functions [21], [15]. These basis functions make it possible to study microstrip circuits of many different geometries [15] and have the advantage that their spectral versions [see (12)] are simple closed-form expressions, which is very important for the efficient computation of $\Gamma_{jl}^{ik}(i, j = 1, 2;\ k = 1, \cdots, N_i;\ l = 1, \cdots, N_j)$ via (7). The mathematical expression of the rooftop basis functions used in this paper is

$$\boldsymbol{j}_{jl}(x, z) = T_x(x - x_{jl}, z - z_{jl})\hat{\boldsymbol{x}}, \quad j = 1, 2;\ l = 1, \cdots, N_{xj} \tag{13}$$

$$\boldsymbol{j}_{jl}(x, z) = T_z(x - x_{jl}, z - z_{jl})\hat{\boldsymbol{z}}, \quad j = 1, 2;\ l = N_{xj} + 1, \cdots, N_{xj} + N_{zj} = N_j \tag{14}$$

where

$$T_x(x, z) = \begin{cases} 1 - \dfrac{|x|}{w_x}, & |x| < w_x,\ |z| < \dfrac{w_z}{2} \\ 0, & \text{elsewhere} \end{cases} \tag{15}$$

$$T_z(x, z) = \begin{cases} 1 - \dfrac{|z|}{w_z}, & |z| < w_z,\ |x| < \dfrac{w_x}{2} \\ 0, & \text{elsewhere.} \end{cases} \tag{16}$$

One more thing that has to be specified before solving the system of linear equations (4) is the expression of the tangential excitation electric field on $S_1$ and $S_2$. As suggested in [17], in this paper, distributed delta-gap voltage generators are used for exciting the two microstrip transmission lines of Fig. 1(b) all along the width of the metallic strips of these two microstrip lines (so that the current density basis functions placed at the excitation planes are all connected in parallel, as shown in [17, Fig. 6]). The mathematical expression for the tangential excitation electric field introduced in $S_1$ and $S_2$ by these distributed delta-gap generators is given by [see Fig. 1(b)]

$$\boldsymbol{E}_{t,\text{exc}}(x, y = d_{M_i}, z) = V_i \delta(z - z_{\text{exc}}^{i})\left[u(x - x_{0i}) - u(x - x_{0i} - w_i)\right]\hat{\boldsymbol{z}}, \quad i = 1, 2 \tag{17}$$

where $V_i (i = 1, 2)$ is the voltage across the delta-gap generator connected to the $i$th $(i = 1, 2)$ transmission line and $u(\bullet)$ is the unit step function ($u(x) = 1$ if $x > 0$ and $u(x) = 0$ if $x < 0$).

For the solution of the system of equations (4), the authors of this paper have used a preconditioned biconjugate gradient method routine [22], which has proven to be fast, stable, and accurate, even in those cases in which several thousand unknowns were involved in the system of equations.

It should be pointed out that although the computational expense required for the determination of $\Gamma_{jl}^{ik}(i, j = 1, 2;\ k = 1, \cdots, N_i;\ l = 1, \cdots, N_j)$ via (7) is much smaller than that required when (5) is used, the CPU time involved in the brute-force numerical computation of $\Gamma_{jl}^{ik}(i, j = 1, 2;\ k = 1, \cdots, N_i;\ l = 1, \cdots, N_j)$ via (7) can be still too high. In the cases in which the two basis functions involved in the computation of $\Gamma_{jl}^{ik}$ belong to the approximation of the current density on metallizations placed at different planes of the multilayered substrate of Fig. 1(a) [i.e., when $i \neq j$ in (7)], the elements of the corresponding spectral Green's function of (7), i.e., $\overline{\tilde{\boldsymbol{G}}}_t(n, y = d_{M_i}, y' = d_{M_j}, k_z)(i \neq j)$, exponentially decay as both $n$ and $k_z$ increase. As a consequence of this, the numerical computation of infinite summations of infinite integrals of (7) does not usually have to be extended to high values of $k_z$ and $n$ when $i \neq j$, which leads to short CPU times. However, the situation completely changes in the cases in which the two basis functions involved in the computation of $\Gamma_{jl}^{ik}$ belong to the approximation of the current density on metallizations placed at the same plane of the multilayered substrate of Fig. 1(a) [i.e., when $i = j$ in (7)] since, in these cases, the elements of the corresponding spectral Green's function of (7), i.e., $\overline{\tilde{\boldsymbol{G}}}_t(n, y = d_{M_i}, y' = d_{M_j}, k_z)(i = j)$, do not decay as both $n$ and $k_z$ increase. As a consequence of this latter fact, the direct application of (7) for the determination of $\Gamma_{jl}^{ik}$ requires that the numerical computation of infinite summations of infinite integrals has to be extended to very high values of $k_z$ and $n$ when $i = j$, which leads to very high CPU times. Bearing in mind all these ideas, whereas in this paper, (7) has been directly used for the determination of $\Gamma_{jl}^{ik}$ in the cases in which $i \neq j$, a special procedure has been designed for the quick computation of $\Gamma_{jl}^{ik}$ in those cases in which $i = j$. In the first step of this procedure, for every value of the summation index $n$, the asymptotic behaviors for high values of $k_z$ of the two matrix functions $\overline{\tilde{\boldsymbol{G}}}_t(n, y = d_{M_i}, y' = d_{M_i}, k_z)(i = 1, 2)$ are interpolated in terms of Chebyshev polynomials of the variable $1/k_z$ [18], [23]. Once this interpolation has been carried out, every infinite integral of (7) in which $i = j$ is split into two integrals, one integral with finite limits containing the matrix function $\overline{\tilde{\boldsymbol{G}}}_t(n, y = d_{M_i}, y' = d_{M_i}, k_z)(i = 1 \text{ or } 2)$ and one integral with infinite limits containing the interpolated version of $\overline{\tilde{\boldsymbol{G}}}_t(n, y = d_{M_i}, y' = d_{M_i}, k_z)(i = 1 \text{ or } 2)$ [see

[23, eqn. (30)]]. The integrals with finite limits are numerically computed within short CPU times and the integrals with infinite limits are determined in closed form in terms of sine and cosine integral functions, as in [23]. In the second step of the procedure, the numerically obtained integrals of (7) are considered to be functions of the summation index $n$, which either exponentially decay for high values of $n$ (thus leading to short CPU times in the computation of the corresponding infinite summations) or show an asymptotic behavior, which can be approximated as the product of sinusoidal functions of $n$ times a Chebyshev polynomial of the variable $1/n$. In the latter case, every infinite summation of (7) is split into a first summation with finite limits amenable to computation within a short CPU time, and a second summation with infinite limits containing the asymptotic behavior of the integrals functions of $n$ (i.e., containing the sinusoidal functions and Chebyshev polynomials), which can be obtained in closed form.

### C. Deembedding of Scattering Parameters

In order to obtain the scattering parameters of the two-port microstrip circuit of Fig. 1(a) and (b), the current density on the metallizations of the circuit and feeding lines has to be obtained for two independent excitations of the circuit [e.g., for the case in which $V_1 = 1$ V and $V_2 = 0$ V in (17), and the case in which $V_1 = 0$ V and $V_2 = 1$ V in (17)] by using the method described above in this section. Once the current density on the strips of the feeding transmission lines is known, it must be integrated along the $x$-coordinate in order to obtain the current flowing across these transmission lines. In the regions of these transmission lines, close to the microstrip circuit and the delta-gap generators, the excited evanescent higher order modes are present in the currents values . However, in the regions of these transmission lines, which are far enough from the microstrip circuit and delta-gap generators, the evanescent higher order modes can be neglected and the currents show a standing-wave pattern consisting of incident and reflected current waves. According to this, if we let $I_i^m(z)$ be the value of the current on the $i$th $(i = 1, 2)$ transmission line at the $m$th excitation $(m = 1, 2)$, in the regions far from the microstrip circuit and the generators, $I_i^m(z)(m = 1, 2; i = 1, 2)$ should admit an expression of the type

$$I_i^m(z) = I_{im}^+ e^{-j\beta_i(z-z_{0i})} + I_{im}^- e^{j\beta_i(z-z_{0i})}, \qquad m = 1, 2;\ i = 1, 2 \tag{18}$$

where $\beta_i$ $(i = 1, 2)$ is the phase constant of the fundamental quasi-TEM mode of the $i$th $(i = 1, 2)$ microstrip transmission line, and $z = z_{01}$ and $z = z_{02}$ are assumed to be the reference planes [see Fig. 1(b)] in which we plan to compute the scattering parameters of the two-port circuit of Fig. 1(a) and (b). In this paper, the authors have made use of (18) for obtaining the complex amplitudes of the incident and reflected current waves $I_{im}^+$ and $I_{im}^-$ $(m = 1, 2;\ i = 1, 2)$, and from these complex amplitudes, the scattering parameters of the two-port circuit. In order to determine $I_{im}^+$ and $I_{im}^-$ $(m = 1, 2;\ i = 1, 2)$, the feeding microstrip lines appearing in Fig. 1(b) have been taken to be 2.25 guided wavelengths long, and the regions of the microstrip lines in which the current waves can be written as in (18) have been assumed to be 1.25 guided wavelengths long, and have been assumed to be separated 0.5 guided wavelengths from the both microstrip circuit and the generators exciting those lines (in [24, Table I], the authors show for a microstrip open-end discontinuity that feeding microstrip lines longer than 2.25 guided wavelengths are not necessary since the results obtained in that case for a feeding line that is 2.25 guided wavelengths long do not appreciable differ from those obtained when the length of the feeding line is increased). In the region in which (18) is assumed to be valid, a set of samples of $I_i^m(z)(m = 1, 2;\ i = 1, 2)$ has been obtained for different values of $z$ by applying Galerkin's method, and then the complex amplitudes $I_{im}^+$ and $I_{im}^-$ $(m = 1, 2;\ i = 1, 2)$ and the phase constants $\beta_i$ $(i = 1, 2)$ of (18) have been fitted to these samples by means of the matrix pencil technique, as explained in [25] and [26]. Once the complex amplitudes $I_{im}^+$ and $I_{im}^-$ $(m = 1, 2;\ i = 1, 2)$ are known, the scattering parameters of the two-port circuit of Fig. 1(a) and (b) can be obtained via standard circuit theory by using the following equation:

$$\begin{pmatrix} S_{11} & S_{12}\sqrt{\dfrac{Z_{02}}{Z_{01}}} \\ S_{21}\sqrt{\dfrac{Z_{01}}{Z_{02}}} & S_{22} \end{pmatrix} = -\begin{pmatrix} I_{11}^- & I_{12}^- \\ I_{21}^+ & I_{22}^+ \end{pmatrix}\begin{pmatrix} I_{11}^+ & I_{12}^+ \\ I_{21}^- & I_{22}^- \end{pmatrix}^{-1} \tag{19}$$

where $Z_{0i}(i = 1, 2)$ is the characteristic impedance of the fundamental mode of the $i$th $(i = 1, 2)$ microstrip transmission line. Since the two-port circuit of Fig. 1(a) and (b) is a reciprocal network, $S_{12} = S_{21}$ in (19), and, as a consequence of this fact, the complex amplitudes $I_{im}^+$ and $I_{im}^-$ $(m = 1, 2;\ i = 1, 2)$ suffice to obtain $S_{ij}(i, j = 1, 2)$ via (19) (i.e., the impedances $Z_{0i}$ are not necessary for the computation of the scattering parameters).

In order to demonstrate the validity of the method followed for the calculation of the scattering parameters, we have always applied two independent tests. The first test has been to verify power conservation (i.e., to verify that $|S_{11}|^2 + |S_{12}|^2 = 1$ since the circuits studied in this paper are lossless and nonradiating). The second test has been to check that the values of the phase constants $\beta_1$ and $\beta_2$ provided by the matrix pencil fitting procedure coincide with those that are obtained via standard two-dimensional analysis [7]. It should be pointed out that these two tests have been successfully passed by all the scattering parameters results that are shown in Section III.

## III. Numerical Results

In Table I, the validity of the numerical method described in Section II is tested by comparing our results for the equivalent-circuit capacitances of open-end microstrip discontinuities on anisotropic substrates with the results obtained for those capacitances in [11]. Our results for every open-circuit capacitance $C_{oc}$ are obtained by means of the formula $C_{oc} = (1/2\pi f Z_0)\tan(|\angle S_{11}|/2)$ in which $f$ is the frequency, $\angle S_{11}$ is the phase of $S_{11}$ computed via the method of Section II, and $Z_0$ is the full-wave characteristic impedance of the corresponding open-ended microstrip line (power–current definition) computed by means of the method described in

TABLE I
NORMALIZED CAPACITANCES OF OPEN-END MICROSTRIP DISCONTINUITIES ON PYROLITIC–BORON–NITRIDE: $\epsilon_{xx} = \epsilon_{zz} = 5.12$, $\epsilon_{yy} = 3.4$ AND SAPPHIRE: $\epsilon_{xx} = \epsilon_{zz} = 9.4$, $\epsilon_{yy} = 11.6$ ($h = 1$ mm, $b = 11h$, $a = 20$ mm WHEN $w/h \leq 2$, $a = 40$ mm WHEN $w/h = 4$, $a = 60$ mm WHEN $w/h = 6$, $f = 2$ GHz)

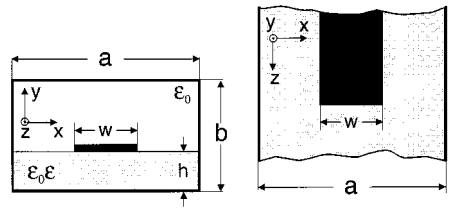


| | $C_{oc}/W$ (pF/m) | | | |
|---|---|---|---|---|
| | $\varepsilon_{xx}=\varepsilon_{zz}=5.12$ $\varepsilon_{yy}=3.4$ | | $\varepsilon_{xx}=\varepsilon_{zz}=9.4$ $\varepsilon_{yy}=11.6$ | |
| W/h | Toncich & Collin | Our results | Toncich & Collin | Our results |
| 0.25 | 43.04 | 42.25 | 80.36 | 82.42 |
| 0.5 | 33.95 | 34.17 | 65.56 | 64.83 |
| 1.0 | 28.27 | 27.90 | 56.38 | 56.68 |
| 2.0 | 24.84 | 24.58 | 50.95 | 51.20 |
| 4.0 | 22.72 | 23.26 | 47.43 | 46.23 |
| 6.0 | 21.66 | 21.99 | 45.35 | 45.18 |

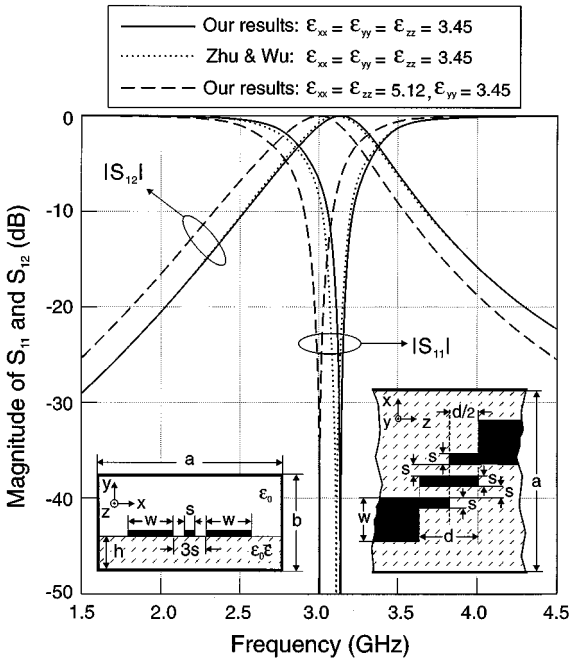


Fig. 2. Return and insertion losses of coupled-line bandpass filter on isotropic pyrolitic–boron–nitride $\epsilon_{xx} = \epsilon_{yy} = \epsilon_{zz} = 3.45$ and anisotropic pyrolitic–boron–nitride: $\epsilon_{xx} = \epsilon_{zz} = 5.12$, $\epsilon_{yy} = 3.45$ ($h = 0.6$ mm, $b = 11h$, $a = 8$ mm, $w = 1.36$ mm, $s = 0.34$ mm, $d = 30.8$ mm). Our results are compared with those published in [28].

[27]. It can be noticed that the discrepancies between our results and those reported in [11] are always within 2.5%, which is a good check for the validity of our method. As an additional test, our results for the frequency-dependence of the normalized input susceptance $2\pi f Z_0 C_{oc} = \tan(|\angle S_{11}|/2)$ of an open-end microstrip discontinuity on anisotropic sapphire have also been compared with those published in [12, Fig. 3] in the frequency range of $0 < f < 20$ GHz (in this latter case, the dimensions of the rectangular waveguide shown in the figure of Table I have been chosen to be $a = 5h = 5$ mm and $b = 6h = 6$ mm). Excellent agreement has been found between the two set of results for frequencies up to 16 GHz. However, it has been noticed that, as the frequency is changed from 16 GHz to 20 GHz, our results are increasingly larger than those of [12], and a maximum difference of 15% occurs at 20 GHz. These latter discrepancies are attributed to the effect (growing with frequency) of radiation losses in the unshielded discontinuity analyzed in [12], which is not present in the shielded discontinuity analyzed with the method of Section II. The comparison between our results and those of [12] is not included in this paper for the sake of brevity.

In Fig. 2, the results published in [28] for the return and insertion losses of a microstrip bandpass filter on an isotropic dielectric substrate are compared with our results. In spite of the fact that the results of [28] have been obtained for a microstrip filter in an open environment and our results have been obtained for a shielded microstrip filter, the agreement between the results of [28] and our results is relatively good. In fact, the difference between the center frequency of the filter predicted in [28] and that predicted by our method is approximately 1%. Also in Fig. 2, comparison is carried out with the results that would be obtained for the microstrip filter if the dielectric substrate were anisotropic with a permittivity value in the direction perpendicular to the air–dielectric interface equal to that of the isotropic substrate used in [28]. It can be checked that the center frequency of the filter predicted by our method in the anisotropic case is 4.5% below that predicted by our method in the isotropic case, which indicates that an erroneous prediction of the center frequency of the filter is made when substrate dielectric anisotropy is neglected.

In Fig. 3, a comparison is carried out between the results published in [4] for the magnitude of the scattering parameters of several overlapping microstrip transitions and our results for the same structures. As it happens with Fig. 2, the results of [4] plotted in Fig. 3 have been obtained for microstrip transitions in an open environment, and our results in Fig. 3 have been obtained for shielded microstrip transitions. Since the level of radiated power in the structures analyzed in [4] is sometimes high (this can be easily verified by computing $|S_{11}|^2 + |S_{12}|^2$ for these structures), the results of [4] sometimes appreciably differ from our results. However, the prediction made in [4] of the value of the overlapping length for which maximum reflection is achieved ($l/\lambda_0 \approx 0.15$) matches pretty well our own prediction. Also in Fig. 3, the authors plot the results obtained for the overlapping microstrip transitions when one of the dielectrics of the two-layered substrate is obliged to be anisotropic by changing its permittivity in the direction parallel to the air–dielectric interface. It is noticed that, in the anisotropic case, the value of the overlapping length for which maximum reflection is achieved is approximately 6% below the value predicted in the isotropic case by the results of [4] and by our own method.

In Fig. 4, results are presented for the insertion losses of a microstrip gap discontinuity manufactured on an anisotropic sub-

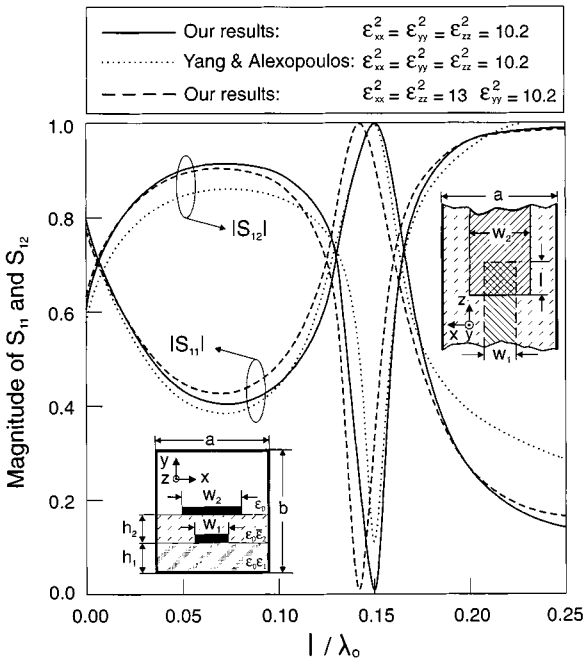


Fig. 3. Return and insertion losses of collinear overlapping microstrip transition on two-layered substrate. Results are presented for isotropic Epsilam-10 layer: $\epsilon^2_{xx} = \epsilon^2_{yy} = \epsilon^2_{zz} = 10.2$ and anisotropic Epsilam-10 layer: $\epsilon^2_{xx} = \epsilon^2_{zz} = 13$, $\epsilon^2_{yy} = 10.2$ ($\epsilon^1_{xx} = \epsilon^1_{yy} = \epsilon^1_{zz} = 2.2$, $h_1 = h_2 = 0.635$ mm, $b = 12h$, $a = 10$ mm, $w_1 = 1.0668$ mm, $w_2 = 1.9304$ mm, $f = 10$ GHz). Our results are compared with those published in [4].

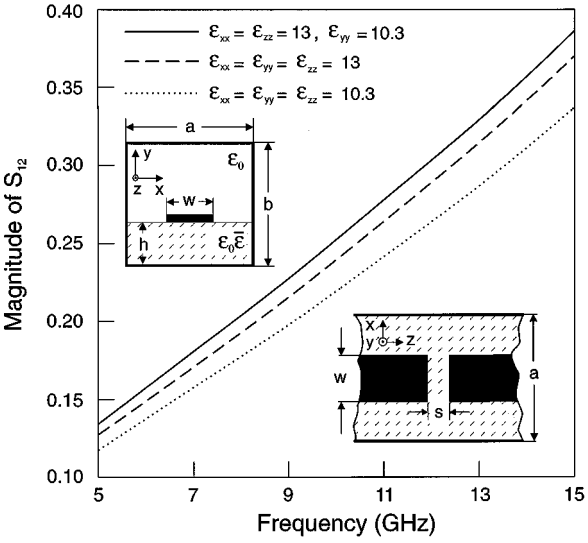


Fig. 4. Insertion losses of microstrip gap discontinuity on isotropic Epsilam-10: either $\epsilon_{xx} = \epsilon_{yy} = \epsilon_{zz} = 13$ or $\epsilon_{xx} = \epsilon_{yy} = \epsilon_{zz} = 10.3$ and anisotropic Epsilam-10: $\epsilon_{xx} = \epsilon_{zz} = 13$, $\epsilon_{yy} = 10.3$ ($h = 0.635$ mm, $b = 11h$, $a = 8$ mm, $w = 0.57$ mm, $s = 0.1$ mm).

strate—Epsilam-10—and these results are compared with the results that would be obtained if the substrate were assumed to be isotropic with both a permittivity value equal to that of Epsilam-10 in the direction parallel to the air–dielectric interface and a permittivity value equal to that of Epsilam-10 in the direction perpendicular to the air–dielectric interface. Whereas

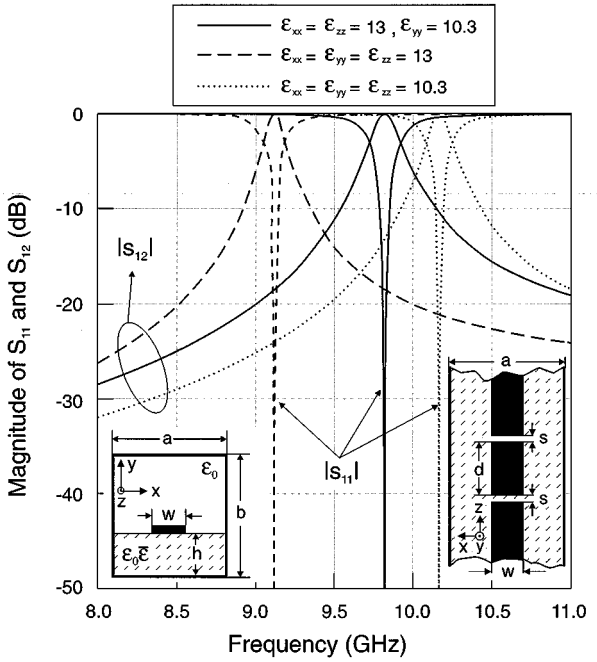


Fig. 5. Return and insertion losses of coupled resonator bandpass filter on isotropic Epsilam-10: either $\epsilon_{xx} = \epsilon_{yy} = \epsilon_{zz} = 13$ or $\epsilon_{xx} = \epsilon_{yy} = \epsilon_{zz} = 10.3$ and anisotropic Epsilam-10: $\epsilon_{xx} = \epsilon_{zz} = 13$, $\epsilon_{yy} = 10.3$ ($h = 0.635$ mm, $b = 11h$, $a = 12.7$ mm, $w = 0.57$ mm, $s = 0.1$ mm, $d = 5$ mm).

the results obtained for the gap on the isotropic substrate with relative permittivity 10.3 are on average 13% below the results obtained for the gap on anisotropic Epsilam-10, the results obtained for the gap on the isotropic substrate with relative permittivity 13 are on average 5% below the results obtained for the gap on anisotropic Epsilam-10. In order to explain the different percentage of discrepancy between the results obtained in the anisotropic case and the results obtained in every isotropic case, it is necessary to take into account that, in the case of the gap discontinuity on anisotropic Epsilam-10, the two microstrip lines involved are tightly coupled (the gap is very narrow) and, as a consequence of this, the portion of electric field in the gap region that sees the permittivity in the direction parallel to the air–dielectric interface is bigger than the portion of electric field that sees the permittivity in the direction perpendicular to the air–dielectric interface. Therefore, the results obtained in the isotropic case using the permittivity of Epsilam-10 in the direction parallel to the air–dielectric interface must accordingly be closer to the results obtained with the real permittivity tensor of Epsilam-10 than the results obtained in the isotropic case using the permittivity of Epsilam-10 in the direction perpendicular to the air–dielectric interface.

In Fig. 5, the scattering parameters of a microstrip bandpass filter containing two microstrip gap discontinuities [29] are computed when the substrate is anisotropic Epsilam-10 and when the substrate is an isotropic dielectric whose permittivity may take the value of any of the two different elements of the permittivity tensor of Epsilam-10. Somehow, the study of Fig. 5 can be viewed as an extension of the study carried out in Fig. 4. In the case of Fig. 5, the results obtained for the filter on the isotropic substrate with the permittivity of Epsilam-10 in the

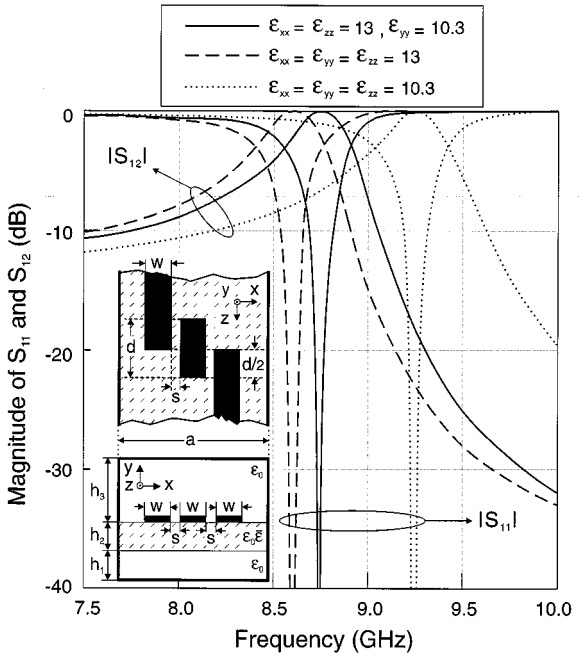


Fig. 6. Return and insertion losses of coupled-line bandpass filter in suspended substrate configuration. Results are presented for isotropic Epsilam-10 layer: either $\epsilon_{xx} = \epsilon_{yy} = \epsilon_{zz} = 13$ or $\epsilon_{xx} = \epsilon_{yy} = \epsilon_{zz} = 10.3$ and for anisotropic Epsilam-10 layer: $\epsilon_{xx} = \epsilon_{zz} = 13$, $\epsilon_{yy} = 10.3$ ($h_1 = h_2 = 0.635$ mm, $h_3 = 10h_1$, $a = 12.7$ mm, $w = 2.1$ mm, $s = 0.7$ mm, $d = 8$ mm).

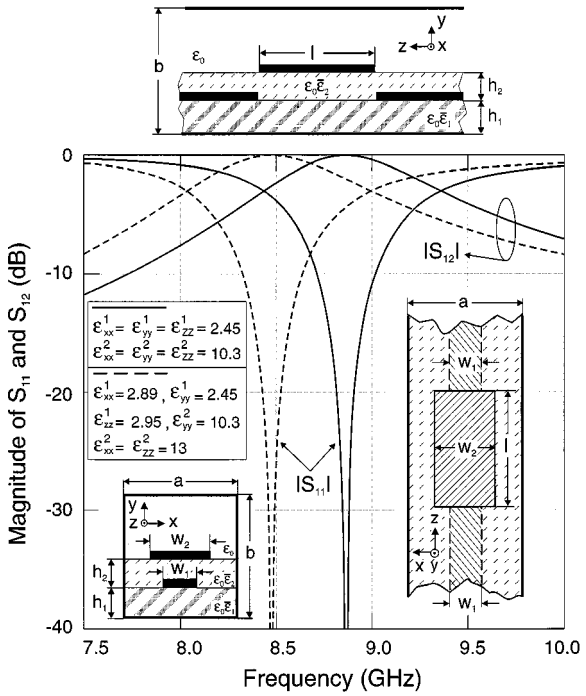


Fig. 7. Return and insertion losses of coupled resonator bandpass filter on two-layered substrate. Results are presented for isotropic PTFE: $\epsilon^1_{xx} = \epsilon^1_{yy} = \epsilon^1_{zz} = 2.45$ and isotropic Epsilam-10: $\epsilon^2_{xx} = \epsilon^2_{yy} = \epsilon^2_{zz} = 10.3$, layers as well as anisotropic PTFE: $\epsilon^1_{xx} = 2.89$, $\epsilon^1_{yy} = 2.45$, $\epsilon^1_{zz} = 2.95$, and anisotropic Epsilam-10: $\epsilon^2_{xx} = \epsilon^2_{zz} = 10.3$, $\epsilon^2_{yy} = 13$ layers ($h_1 = h_2 = 0.635$ mm, $b = 12h_1$, $a = 12.7$ mm, $w_1 = 0.9$ mm, $w_2 = 1.6$ mm, $l = 6.75$ mm).

direction perpendicular to the air–dielectric interface are closer to the results obtained for the filter on anisotropic Epsilam-10 than the results obtained for the filter on the isotropic substrate with the permittivity of Epsilam-10 in the direction parallel to the air–dielectric interface. In fact, whereas the center frequency predicted for the filter on the isotropic substrate with relative permittivity 10.3 is 4% above that predicted for the filter on anisotropic Epsilam-10, the center frequency predicted for the filter on the isotropic substrate with relative permittivity 13 is 7% below that predicted for the filter on anisotropic Epsilam-10. This indicates that, in the case of the filter on anisotropic Epsilam-10 studied in Fig. 5, the portion of the electric field in the whole filter region (including the microstrip resonator of length $d$ plus the two gap discontinuities) that sees the permittivity in the direction perpendicular to the air–dielectric interface is bigger than the portion of electric field that sees the permittivity in the direction parallel to the air–dielectric interface.

In Fig. 6, the study carried out in Figs. 4 and 5 is repeated for a coupled-line microstrip filter in a suspended substrate configuration. As it happens with Fig. 4, in Fig. 6 the results obtained for the filter on the isotropic substrate with the permittivity of Epsilam-10 in the direction parallel to the air–dielectric interface are closer to the results obtained for the filter on anisotropic Epsilam-10 than the results obtained for the filter on the isotropic substrate with the permittivity of Epsilam-10 in the direction perpendicular to the air–dielectric interface. Thus, whereas the center frequency predicted for the filter on the isotropic substrate with relative permittivity 13 is 2% below that predicted for the filter on anisotropic Epsilam-10, the center frequency predicted for the filter on the isotropic substrate with relative permittivity 10.3 is 5.5% above that predicted for the filter on anisotropic Epsilam-10. This indicates that, in the case of the filter on anisotropic Epsilam-10 studied in Fig. 6, the portion of electric field in the whole filter region (including the microstrip resonator of length $d$ plus the two sections of length $d/2$ of feeding microstrip lines coupled to the resonator) that sees the permittivity in the direction parallel to the air–dielectric interface is bigger than the portion of electric field that sees the permittivity in the direction perpendicular to the air–dielectric interface.

In Fig. 7, two sets of results are presented for a microstrip filter containing metallizations at two different levels [3]. The first set of results corresponds to a filter fabricated on a two-layered substrate consisting of one uniaxial anisotropic dielectric—Epsilam-10—and one biaxial anisotropic dielectric—woven glass PTFE. The second set of results also corresponds to a filter fabricated on a two-layered substrate consisting of isotropic dielectrics whose permittivities coincide with the permittivities of the aforementioned anisotropic dielectrics in the direction perpendicular to the air–dielectric interface. Fig. 7 clearly shows that the effects of dielectric anisotropy are appreciable even in the case of filters with metallizations at two different levels. Thus, the center frequency of the filter fabricated with anisotropic dielectrics turn out to be 4.5% below that of the filter fabricated with isotropic dielectrics.

## IV. Conclusions

A numerical algorithm has been developed for the full-wave analysis of two-port shielded microstrip circuits embedded in multilayered substrates with dielectric anisotropy. In this algorithm, the Galerkin's method in the spectral domain is used for determining the current density excited on the metallizations of the circuits by delta-gap voltage generators, and the matrix pencil technique is subsequently applied for deembedding the scattering parameters from the computed current densities. Results obtained for microstrip discontinuities and microstrip filters fabricated on anisotropic dielectrics show that errors around 5% may be made in the computation of the scattering parameters of those discontinuities and filters when dielectric anisotropy is neglected. In the case of circuits fabricated on uniaxial anisotropic dielectrics, it is shown that the response of a circuit on an anisotropic dielectric is sometimes closer to the response obtained for that circuit when it is fabricated on an isotropic dielectric with the permittivity of the anisotropic dielectric in the direction parallel to the air–dielectric interface, and sometimes closer to the response obtained for that circuit when it is fabricated on an isotropic dielectric with the permittivity of the anisotropic dielectric in the direction perpendicular to the air–dielectric interface.

## Acknowledgment

The authors would like to thank Dr. G. Cano, Department of Applied Physics, University of Seville, Seville, Spain, and Dr. F. Medina, Department of Electronics and Electromagnetism, University of Seville, Seville, Spain, for providing a code for the computation of the propagation constant and characteristic impedance of microstrip lines in multilayered substrates with dielectric anisotropy. The authors would also like to thank Dr. O. Pereira, Instituto Tecnologico de Aeronautica, São Paulo State, São Paulo, Brazil, for his many helpful suggestions.

## References

[1] W. Schwab and W. Menzel, "On the design of planar microwave components using multilayer structures," *IEEE Trans. Microwave Theory Tech.*, vol. 40, pp. 67–72, Jan. 1992.

[2] E. K. L. Yeung, J. C. Beal, and Y. M. M. Antar, "Multilayer microstrip structure analysis with matched load simulation," *IEEE Trans. Microwave Theory Tech.*, vol. 43, pp. 143–149, Jan. 1995.

[3] M. J. Tsai, F. De Flaviis, O. Fordham, and N. G. Alexopoulos, "Modeling planar arbitrarily shaped microstrip elements in multilayered media," *IEEE Trans. Microwave Theory Tech.*, vol. 45, pp. 330–337, Mar. 1997.

[4] H. Y. Yang and N. G. Alexopoulos, "Basic blocks for high-frequency interconnects: Theory and experiment," *IEEE Trans. Microwave Theory Tech.*, vol. 36, pp. 1258–1264, Aug. 1988.

[5] N. G. Alexopoulos, "Integrated-circuit structures on anisotropic substrates," *IEEE Trans. Microwave Theory Tech.*, vol. MTT-33, pp. 847–881, Oct. 1985.

[6] D. M. Pozar, "Radiation and scattering from a microstrip patch on a uniaxial substrate," *IEEE Trans. Antennas Propagat.*, vol. AP-35, pp. 613–621, June 1987.

[7] F. Medina, M. Horno, and H. Baudrand, "Generalized spectral analysis of planar lines on layered media including uniaxial and biaxial dielectric substrates," *IEEE Trans. Microwave Theory Tech.*, vol. 37, pp. 504–511, Mar. 1989.

[8] Y. Chen and B. Beker, "Study of microstrip step discontinuities on bianisotropic substrates using the method of lines and transverse resonance technique," *IEEE Trans. Microwave Theory Tech.*, vol. 42, pp. 1945–1950, Oct. 1994.

[9] J. Martel, R. R. Boix, and M. Horno, "Static analysis of microstrip discontinuities using the excess charge density in the spectral domain," *IEEE Trans. Microwave Theory Tech.*, vol. 39, pp. 1623–1631, Sept. 1991.

[10] ——, "Analysis of a microstrip crossover embedded in a multilayered anisotropic and lossy media," *IEEE Trans. Microwave Theory Tech.*, vol. 42, pp. 424–432, Mar. 1994.

[11] S. S. Toncich, R. E. Collin, and K. B. Bhasin, "Full-wave characterization of microstrip open end discontinuities patterned on anisotropic substrates using potential theory," *IEEE Trans. Microwave Theory Tech.*, vol. 41, pp. 2067–2073, Dec. 1994.

[12] J. C. Goswami, A. K. Chan, and C. K. Chui, "Spectral domain analysis of single and coupled microstrip open discontinuities with anisotropic substrates," *IEEE Trans. Microwave Theory Tech.*, vol. 44, pp. 1174–1178, July 1996.

[13] P. B. Katehi and N. G. Alexopoulos, "Frequency-dependent characteristics of microstrip discontinuities in millimeter-wave integrated circuits," *IEEE Trans. Microwave Theory Tech.*, vol. MTT-33, pp. 1029–1035, Oct. 1985.

[14] T. Itoh, "Analysis of microstrip resonators," *IEEE Trans. Microwave Theory Tech.*, vol. MTT-22, pp. 946–952, Nov. 1974.

[15] W. Wertgen and R. H. Jansen, "Efficient direct and iterative electrodynamic analysis of geometrically complex MIC and MMIC structures," *Int. J. Numer. Modeling*, vol. 2, pp. 153–186, 1989.

[16] A. Hill, J. Burke, and K. Kottapalli, "Three-dimensional electromagnetic analysis of shielded microstrip circuits," *Int. J. Microwave Millimeter-Wave Computer-Aided Eng.*, vol. 2, pp. 286–296, 1992.

[17] G. V. Eleftheriades and J. R. Mosig, "On the network characterization of planar passive circuits using the method of moments," *IEEE Trans. Microwave Theory Tech.*, vol. 44, pp. 438–445, Mar. 1996.

[18] R. R. Boix, N. G. Alexopoulos, and M. Horno, "Efficient numerical computation of the spectral transverse dyadic Green's function in stratified anisotropic media," *J. Electromag. Waves Appl.*, vol. 10, no. 8, pp. 1047–1083, 1996.

[19] K. Kawano, "Hybrid-mode analysis of coupled microstrip-slot resonators," *IEEE Trans. Microwave Theory Tech.*, vol. MTT-33, pp. 38–43, Jan. 1985.

[20] F. L. Mesa, R. Marques, and M. Horno, "A general algorithm for computing the bidimensional spectral Green's dyad in multilayered complex bianisotropic media: The equivalent boundary method," *IEEE Trans. Microwave Theory Tech.*, vol. 39, pp. 1640–1649, Sept. 1991.

[21] A. W. Glisson and D. R. Wilton, "Simple and efficient numerical methods for problems of electromagnetic radiation and scattering from sources," *IEEE Trans. Antennas Propagat.*, vol. AP-28, pp. 593–603, Sept. 1980.

[22] W. H. Press, S. A. Teukolsky, W. T. Vetterling, and B. P. Flannery, *Numerical Recipes in FORTRAN—The Art of Scientific Computing*, 2nd ed. Cambridge, U.K.: Cambridge Univ. Press, 1992.

[23] V. Losada, R. R. Boix, and M. Horno, "Resonant modes of circular microstrip patches in multilayered substrates," *IEEE Trans. Microwave Theory Tech.*, vol. 47, pp. 488–498, Apr. 1999.

[24] E. Drake, R. R. Boix, M. Horno, and T. K. Sarkar, "Comparison among different approaches for the full-wave MOM characterization of open-ended microstrip lines," *Microwave Opt. Technol. Lett.*, vol. 21, pp. 246–248, 1999.

[25] Y. Hua and T. K. Sarkar, "Matrix pencil method for estimating parameters of exponentially damped/undamped sinusoids in noise," *IEEE Trans. Acoust., Speech, Signal Processing*, vol. 33, pp. 814–824, May 1990.

[26] T. K. Sarkar, Z. A. Maricevic, and M. Kahrizi, "An accurate de-embedding procedure for characterizing discontinuities," *Int. J. Microwave Millimeter-Wave Computer-Aided Eng.*, vol. 2, pp. 135–143, 1992.

[27] G. Cano, F. Medina, and M. Horno, "Characteristic impedances of microstrip and finline with uniaxial or biaxial anisotropic substrates," *Electron. Lett.*, vol. 24, no. 19, pp. 1211–1212, 1988.

[28] L. Zhu and K. Wu, "Characterization of unbounded multiport microstrip passive circuits using an explicit-network based method of moments," *IEEE Trans. Microwave Theory Tech.*, vol. 45, pp. 2114–2124, Dec. 1997.

[29] U. V. Gothelf and A. Ostegaard, "Full-wave analysis of a two slot microstrip filter using a new algorithm for computation of the spectral integrals," *IEEE Trans. Microwave Theory Tech.*, vol. 41, pp. 101–108, Sept. 1993.

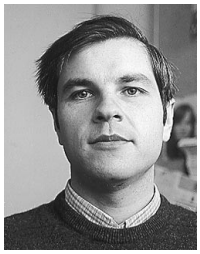

**Enrique Drake** was born in Montilla, Córdoba, Spain, in 1966. He received the Licenciado and Doctor degrees in physics from the University of Seville, Seville, Spain, in 1989 and 1995 respectively.

Since 1992, he has been with the Applied Physics Department, University of Seville, where, in 1999, he became an Associate Professor. His research interests include the numerical analysis of planar transmission lines and circuits.

**Rafael R. Boix** (M'97) was born in Melilla, Spain, in 1962. He received the Licenciado and Doctor degrees in physics from the University of Seville, Seville, Spain, in 1985 and 1990, respectively.

Since 1985, he has been with the Electronics and Electromagnetics Department, University of Seville, where, in 1994, he became an Associate Professor. During the summers of 1991 and 1992, he was with the Electrical Engineering Department, University of California at Los Angeles, as a Visiting Scholar. During the summer of 1996, he was with the Electrical and Computer Engineering Department, Syracuse University, Syracuse, NY, as a Visiting Scholar. His current research interest is focused on the analysis of the effects of complex substrates on the performance of planar transmission-line discontinuities, planar passive microwave circuits, planar resonators, and printed circuit antennas.

**Manuel Horno** (M'75) was born in Torre del Campo, Jaen, Spain in 1947. He received the Licenciado and Doctor degrees in physics from the University of Seville, Seville, Spain, in 1969 and 1972, respectively.

From 1969 to 1986, he was with the Department of Electronics and Electromagnetics at the University of Seville, where he became an Associate Professor (1975) and Full Professor (1986). His research focused on the solution of boundary value problems in electromagnetic theory, wave propagation through anisotropic media, and microwave integrated circuits. During the last few years, he was engaged in the analysis of planar transmission lines embedded in complex materials, synthesis of passive microwave circuits containing planar transmission lines, and characterization of planar transmission-line discontinuities and printed antennas. He died in September 1998, in Seville, Spain.

Prof. Horno was a member of the Electromagnetic Academy of the Massachusetts Institute of Technology, Cambridge.

**Tapan K. Sarkar** (S'69–M'76–SM'81–F'92) received the B.Tech. degree from the Indian Institute of Technology, Kharagpur, India, the M.Sc.E. degree from the University of New Brunswick, Fredericton, NB, Canada, in 1969, and the M.S. and Ph.D. degrees from Syracuse University, Syracuse, NY, in 1971 and 1975, respectively.

From 1975 to 1976, he was with the TACO Division, General Instruments Corporation. From 1976 to 1985, he was with the Rochester Institute of Technology, Rochester, NY. From 1977 to 1978, he was a Research Fellow at the Gordon McKay Laboratory, Harvard University, Cambridge, MA. He is currently a Professor in the Department of Electrical and Computer Engineering, Syracuse University. He has authored or co-authored over 180 journal papers and has written chapters in eight books. His current research interests deal with numerical solutions of operator equations arising in electromagnetics and signal processing with application to system design.

Dr. Sarkar is a Registered Professional Engineer in the State of New York. He is a member of Sigma Xi and the International Union of Radio Science Commissions A and B. He was an associate editor for feature articles of the *IEEE Antennas and Propagation Society Newsletter*. He was the technical program chairman for the 1988 IEEE AP-S International Symposium and URSI Radio Science Meeting, and has been appointed U.S. research council representative to many URSI General Assemblies. He is the chairman of the Intercommission Working Group of International URSI on Time-Domain Metrology. He received one of the 1977 "Best Solution" Awards presented at the Rome Air Development Center (RADC) Spectral Estimation Workshop, the 1979 Best Paper Award of the IEEE TRANSACTIONS ON ELECTROMAGNETIC COMPATABILITY, and a 1997 Best Paper Award presented at the National Radar Conference (NATRAD'97).